Geophysical Research Letters

RESEARCH LETTER
10.1029/2019GL084919

Key Points:
- Low-energy photoelectrons on the Martian dayside have pitch angle distributions consistent with conservation of adiabatic invariants
- High-energy electrons on the Martian dayside have a flux peak at perpendicular pitch angles, indicating a ubiquitous energization process
- Wave-particle interactions are the most likely candidate to produce such distributions for high-energy electrons

Supporting Information:
- Supporting Information S1

Correspondence to:
A. Shane,
adshane@umich.edu

Citation:
Shane, A., Liemohn, M., Florie, C., & Xu, S. (2019). Misbehaving high-energy electrons: Evidence in support of ubiquitous wave-particle interactions on dayside Martian closed crustal magnetic fields. *Geophysical Research Letters*, *46*, 11,689–11,697. https://doi.org/10.1029/2019GL084919

Received 8 AUG 2019
Accepted 5 OCT 2019
Accepted article online 17 OCT 2019
Published online 7 NOV 2019

Misbehaving High-Energy Electrons: Evidence in Support of Ubiquitous Wave-Particle Interactions on Dayside Martian Closed Crustal Magnetic Fields

Alexander Shane[1], Michael Liemohn[1], Corinne Florie[1], and Shaosui Xu[2]

[1]Department of Climate and Space Sciences and Engineering, University of Michigan, Ann Arbor, MI, USA, [2]Space Sciences Laboratory, University of California, Berkeley, CA, USA

Abstract Multiple studies have reported either isotropic or trapped pitch angle distributions of high-energy (>100 eV) electrons on closed crustal field lines on the dayside of Mars. These pitch angle distributions are not to be expected from collisional scattering and conservation of adiabatic invariants alone. We use 2 years of data from the Mars Atmosphere and Volatile EvolutioN mission to analyze the pitch angle distributions of superthermal electrons on dayside-closed crustal magnetic fields and compare to results from an electron transport model. Low-energy electrons (10–60 eV) have pitch angle distributions in agreement with modeling results, while high-energy electrons (100–500 eV) do not. High-energy electrons have a flux peak at perpendicular pitch angles which suggests there is a ubiquitous energization process occurring on crustal fields. Wave-particle interactions seem to be the most likely candidate. Trapping of high-energy electrons may impact the nightside ionosphere dynamics.

Plain Language Summary Superthermal electrons are electrons with energies between 1 and 1,000 eV and can be produced from ionizing a neutral atmospheric molecule (photoelectron). These electrons are efficient at shifting energy around in space environments due to their high speeds and their ability to interact with the more ubiquitous lower energy (thermal) plasma. Past studies have investigated the distribution of photoelectrons on the crustal magnetic fields of Mars, and they do not always agree with past modeling results and a basic understanding of electron transport. In this study, we use data from the Mars Atmosphere and Volatile EvolutioN mission in order to understand the distribution of these electrons throughout the Mars space environment, previously impossible due to spacecraft orbits. We find that the lower energy electrons (10–60 eV) behave as expected but the higher-energy electrons (100–500 eV) do not. We find that the type of distribution statistically seen by Mars Atmosphere and Volatile EvolutioN for these high-energy electrons suggests that a ubiquitous energization process is occurring on the dayside crustal magnetic fields of Mars. We consider multiple physical processes capable of producing such observed distributions and conclude that wave-particle interactions are the most likely candidate.

1. Introduction/Motivation

Superthermal electrons (1–1,000 eV) are an important population of particles common throughout the solar system. They are excellent at shifting energy from one place to another in space environments through interactions with the bulk thermal plasma. Photoelectrons are one population of superthermal electrons, produced through ionization of neutral particles, and have been studied extensively at Earth, Mars, and Venus and even moons such as Titan (see Coates et al., 2011, for a review). Photoelectrons have a distinct energy spectrum that allows them to be readily identified in the data. One characteristic of the photoelectron energy spectrum includes flux peaks in the 20- to 30-eV range determined by the dominant atmospheric neutrals. At Mars, the primary peaks occur at 22.29 eV (O) and at 22.69 and 27.02 eV (CO_2). Other unique features of the photoelectron energy spectrum at Mars include the "photoelectron knee" at ~60 eV as a result in a drop in ionizing solar radiation (a characteristic shared by photoelectrons at other solar system bodies as well), a flux peak due to carbon Auger electrons at ~250 eV visible in measurements during times of intense photoelectron fluxes Xu et al. (2018) and another flux peak at 500 eV due to oxygen Auger electrons. These distinct spectral features have allowed studies of the Mars space environment such as Xu et al. (2014), Shane et al. (2016), and Xu et al. (2017) to determine whether a measurement is observing photoelectrons or solar wind electrons.

Pitch angle distributions (PADs; Brain et al., 2007; Weber et al., 2017) and energy spectra (Frahm, Sharber, et al., 2006; Frahm, Winningham, et al., 2006; Liemohn et al., 2006) of superthermal electrons can be used to infer magnetic topology. More recently, Xu et al. (2017, 2019) have utilized both to more accurately determine the magnetic topology in the Mars space environment. Liemohn et al. (2003) used a superthermal electron transport model (Khazanov et al., 1993; Khazanov & Liemohn, 1995; Xu & Liemohn, 2015) to perform data-model comparisons with Mars Global Surveyor (MGS) observations, and at low energies (<100 eV), the model-calculated PADs agreed with MGS results. However, MGS measured isotropic PADs for electrons with >100 eV, while the model calculated a source cone PAD at these energies. This was a case study comparison, and it demonstrated that the model is missing a physical process that produced the observed MGS measurement. Brain et al. (2007) performed a statistical study of 115 eV PADs with MGS data and found that on the dayside, isotropic and trapped (two-sided loss cone) distributions are common on closed crustal field lines, in agreement with the case study of Liemohn et al. (2003). It should be noted that Brain et al. (2007) was using PADs to classify magnetic topology; however, a source cone distribution was not among the common distributions used to do so. In fact, they reported that only 2.8% of the PADs they used on the dayside had a two-sided source cone. These studies suggest that there are unstudied physical processes producing isotropic and trapped distributions on closed crustal field lines, as conservation of adiabatic invariants and collisional scattering predicts a source cone distribution. More recently, Soobiah et al. (2014) observed field-aligned low-energy electrons and trapped high-energy electrons inside of an ionospheric flux rope and, during times of radial field lines, with low-energy PADs that indicate they are open. The electron impact ionization cross sections for the primary upper atmosphere neutral species, CO_2 and O, peak around 100 eV (Itikawa, 2002; Thompson et al., 1995). Therefore, any pitch angle scattering or energy diffusion affecting electrons at these energies will affect the ionosphere below.

The work done by Liemohn et al. (2003) revealed the need to study the PADs of superthermal electrons on closed field lines at Mars. Brain et al. (2007) furthered this need by reporting that the dominant PAD on dayside-closed crustal fields for electrons with 115 eV were isotropic and trapped distributions. However, the Brain et al. (2007) study used MGS data that was locked in an orbit at roughly 400 km and 2 a.m./p.m. local time. This study takes advantage of the precessing elliptical orbit of the Mars Atmosphere and Volatile EvolutioN (MAVEN) mission (Jakosky et al., 2015), which allows sampling of the different regions of the Martian space environment in order to better understand the physics that control the superthermal electron PADs on dayside-closed crustal field lines.

2. Data and Filtering

Over 2 years of data collected from the Solar Wind Electron Analyzer (Mitchell et al., 2016) and Magnetometer (Connerney et al., 2015) spanning the time range 1 December 2014 to 30 December 2016 are used in this study to obtain a clearer picture of the behavior of photoelectrons on dayside-closed crustal field lines. Each PAD is mapped onto a common pitch angle grid of 18 bins each with bin width of 10°. We limit ourselves to energies below 500 eV as there are few photoelectrons with energies greater than this.

Modified pitch angles (Xu et al., 2014; Shane et al., 2016) are used to provide more information about the direction that the electrons are traveling, specifically if the electrons are directed toward or away from the planet. If the magnetic elevation angle is greater than zero, the pitch angles are flipped (i.e., modified pitch angle = 180°− pitch angle, if $B_{\text{elev}} > 0$). Electrons with modified pitch angles of 0–90° have some guiding-center velocity component in the direction of the planet, and electrons with modified pitch angles of 90–180° have some guiding-center velocity component directed away from the planet.

In order to ensure that the measurements being used are observing electrons on dayside-closed field lines and not other field line topographies, multiple filtering criteria are enforced. First, a lower altitude limit is set to 200 km to only include measurements above the photoelectron exobase where the electrons are magnetized (Xu et al., 2016). Second, the solar zenith angle is required to be less than 90° to include only dayside observations. We also require that the shape parameter (Xu et al., 2017) in both source cones is required to be less than one. This criterion is used to filter for closed crustal magnetic fields by examining the low-energy (20–80 eV) and field-aligned (0–30, 150–180 pitch angle) electron energy spectrum. No information of higher-energy electrons and those with perpendicular pitch angles is used. However, this only indicates that the "ends" of the magnetic field lie below the superthermal electron exobase. While this is true for all closed crustal field structures, draped field lines deeply embedded in the ionosphere may also

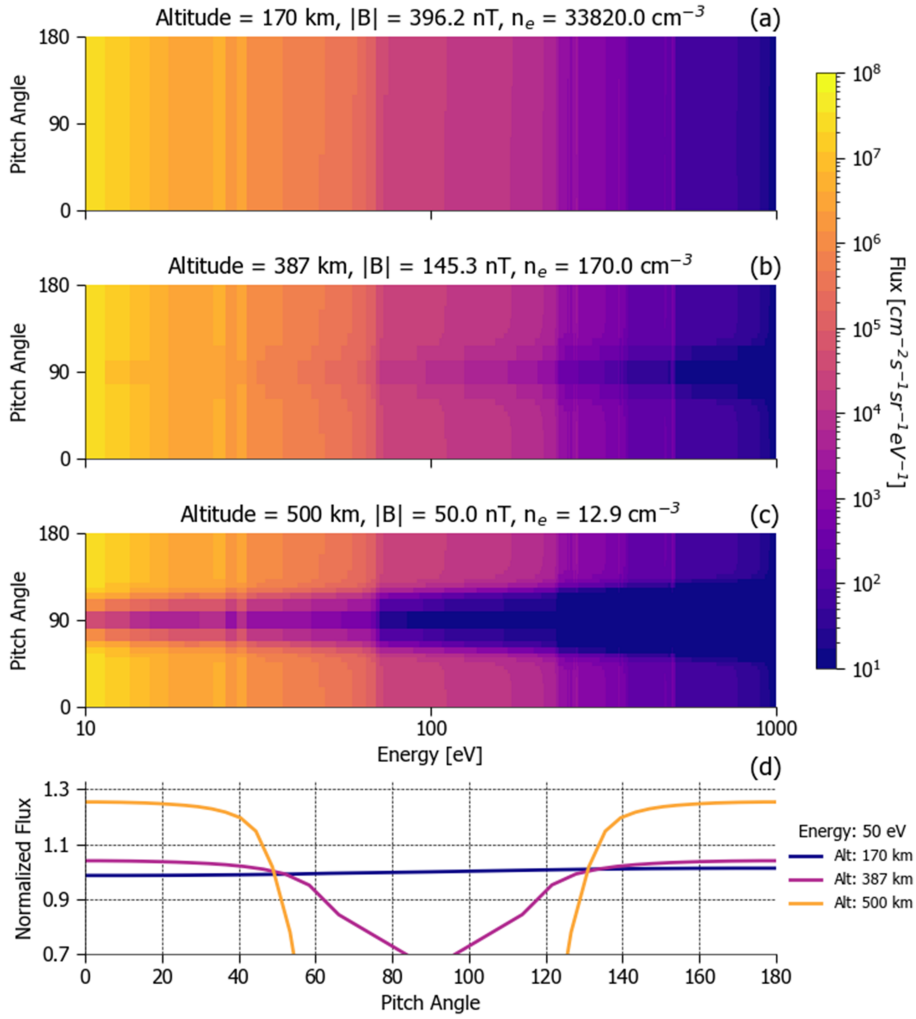

Figure 1. Superthermal electron transport model results of photoelectron pitch angle distributions at three representative locations along a crustal dipole-like magnetic field line: (a) near the exobase, (b) above the exobase, and (c) at the top of the field line. (d) Normalized pitch angle distributions for electrons with energy = 50 eV at each altitude.

share this characteristic. Therefore, a fourth criteria is set that the magnetic field magnitude must be greater than 20 nT to attempt to avoid this scenario. This is by no means a perfect filter, but a higher threshold would start to exclude crustal fields. Lastly, to avoid spacecraft potential issues, a filter is set to only include data when the spacecraft potential (calculated using publicly available MAVEN software) is between −1 and +3 V. After filtering, the data set includes ~296,000 PAD observations each with accompanying magnetic field and ephemeris information.

3. Expected Distribution With Only Collisional Scattering: Model Results

A superthermal electron transport model (STET; Khazanov et al., 1993; Khazanov & Liemohn, 1995; Liemohn et al., 2003; Xu & Liemohn, 2015) is utilized to demonstrate the expected dayside superthermal photoelectron distribution on a closed dipole-like symmetric crustal field line with collisions as the only scattering process. The types of collisions included in the model are collisions with thermal electrons and ions, elastic collisions with neutrals, inelastic excitation scattering with neutrals, and inelastic ionization scattering with neutrals. Figure 1 shows the PADs of superthermal electrons at multiple locations along a field line at 45° solar zenith angle: near the superthermal electron exobase (Figure 1a), a position well above the exobase (Figure 1b), and at the top of the field line (Figure 1c). Below and near the exobase, collisions dominate, and electrons are isotropic in pitch angle regardless of energy (Figure 1a). Above the exobase,

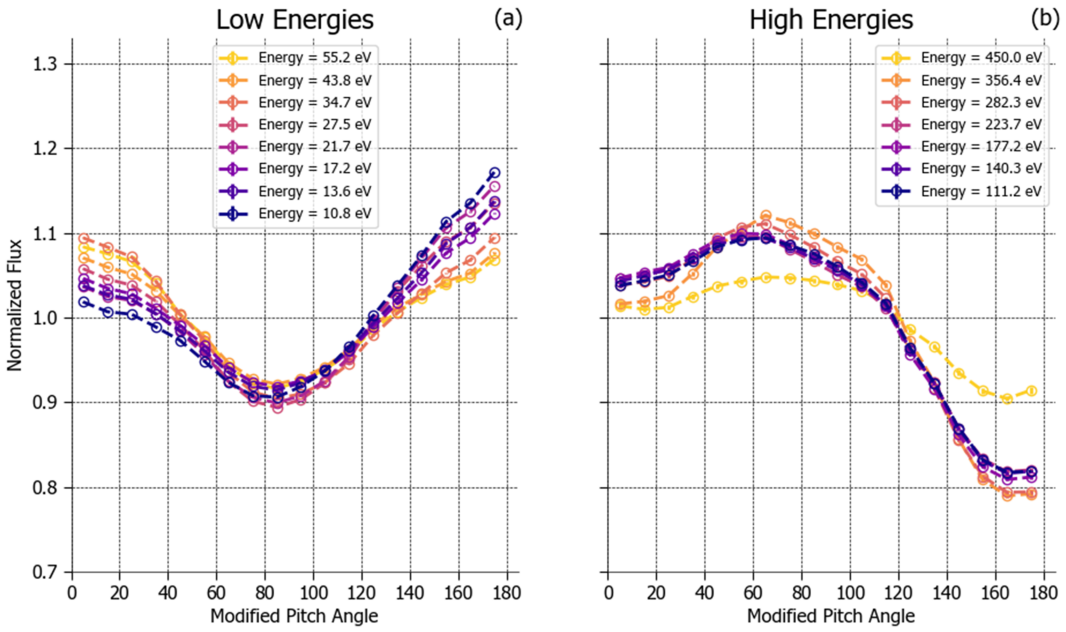

Figure 2. Normalized pitch angle distributions of photoelectrons for (a) low and (b) high energies. The error bars include both measurement and statistical sources of error and are contained within each data marker.

the electrons are magnetized, and collisions play a reducing role as the altitude increases. Collision frequencies (Coulomb and elastic collisions with neutrals) are proportional to E^{-2} where E is the energy of the electron, and this effect can be seen in Figure 1b and more noticeably in Figure 1c. It is easier to see in Figure 1c because the more pronounced source cone allows any scattering into the trapped region to be more noticeable. As an electron travels up the field line, the magnetic field strength decreases. In order to conserve the first adiabatic invariant, the pitch angle of the electron becomes more field aligned producing the anisotropy seen in Figures 1b and 1c. Figure 1d plots the normalized PAD for photoelectrons with $E = 50$ eV at each altitude (vertical slices at 50 eV through each plot). The source cone is more pronounced as altitude increases, that is, the ratio of field-aligned flux to perpendicular flux increases with altitude. This is due to the combined effects of adiabatic invariant conservation and the insignificance of collisions at high altitudes. Different energy electrons will have the same trend in altitude, and higher-energy electrons will experience more anisotropy as collisional effects are less important. The y axis scale used here in Figure 1d is chosen to match the rest of this paper for easier comparison. The normalized flux value at pitch angle = 90° and at altitude = 500 km drops to 0.0025.

Note that these PADs will change with solar conditions, atmospheric densities, and/or magnetic field configurations. The specific magnetic field strengths and background thermal electron densities used are given above each subplot. Different solar conditions and atmospheric densities will move the location of the exobase, affecting where collisions play an important role in controlling the PADs of photoelectrons. Altering the magnetic field configuration may have multiple effects. The ratio of B_{local} and $B_{exobase}$ determines the size of the source cone at any given location along the field line. A field line that is longer horizontally will force electrons to travel longer distances through high-density parts of the atmosphere allowing for more collisions. However, none of these changes will affect the trends in altitude or energy described above. Only the magnitude of the fluxes will be changed and the degree to which the PADs evolve in altitude/energy. We will use this representative example as a baseline, and any deviation seen in the data implies missing physics in the model and a lack of understanding of the Martian space environment.

4. Statistical Results

4.1. Energy Dependence

Figure 2 shows the average normalized PAD over the 2-year filtered data set for low energies (10–60 eV; Figure 2a) and high energies (100–500 eV; Figure 2b). Each curve in Figure 2 is normalized by the average flux in that energy channel over the 2-year period. Both measurement and statistical errors are accounted

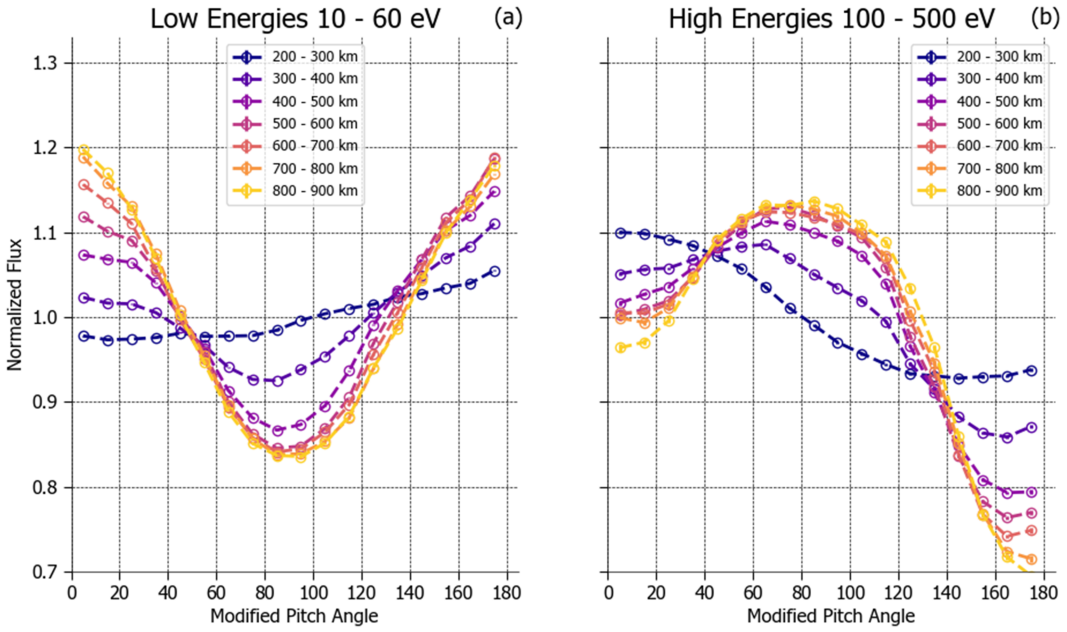

Figure 3. Normalized pitch angle distributions of (a) low- and (b) high-energy photoelectrons as a function of altitude. The error bars include both measurement and statistical sources of error and are contained within each data marker.

for, but due to the large sample size, these errors are small and within the circle markers. The dichotomy between low and high energies is evident from the figure. Low-energy photoelectrons, on average, have a source cone distribution. From section 3, this is what we would expect on a closed crustal field line with only collisional scattering. STET predicts that high-energy photoelectrons should have a more pronounced source cone distribution. Instead, the high-energy photoelectrons measured by MAVEN have a peak in flux at perpendicular pitch angles. Previously, Liemohn et al. (2003) suggested that an energy-dependent pitch angle scattering process is responsible for producing the isotropic high-energy distributions seen by MGS. These results indicate otherwise, as pitch angle scattering processes will isotropize the distribution, not produce a peak at perpendicular pitch angles. One method of forming this distribution is on the nightside of Mars as the crustal field foot points are no longer sunlit, and therefore, the source of electrons has been removed (loss cone distribution). The photoelectrons at field-aligned pitch angles are lost first through energy transfer with the thermal population, and only the trapped particles remain (Shane et al., 2016). However, we have filtered for dayside observations where the source cone is filled with photoelectrons. Therefore, there must be an energization process occurring ubiquitously in the Martian ionosphere/magnetosphere in order to produce the average distribution observed for high-energy photoelectrons. Another interesting feature to note is the asymmetry about 90° pitch angle. There are more high-energy electrons with a velocity component toward the planet than away from it.

4.2. Altitude Dependence

Figure 3 shows how the normalized energy-averaged PADs change with altitude for low- (Figure 3a) and high-energy (Figure 3b) photoelectrons. Flux measurements in each energy channel are normalized by the average flux for that energy for all measurements in each altitude range. The energy channels are then averaged together to produce the curves shown. Low-energy photoelectrons at altitudes just above the exobase (200–300 km) are close to being isotropic. As the altitude increases, the average PAD of low-energy photoelectrons changes from isotropic to a source cone distribution. This source cone distribution becomes more distinct the higher the altitude, in agreement with the results from section 3. High-energy photoelectrons are also close to being isotropic at low altitudes. However, there is an asymmetry about 90° with more high-energy electrons that have a velocity component toward the planet. At higher altitudes, the PAD of high-energy photoelectrons becomes perpendicularly peaked, while the ratio of perpendicular flux to field-aligned flux gets larger. Additionally, the asymmetry about 90° pitch angle also gets bigger the higher the altitude. Of course, these statistical results combine measurements from many magnetic field lines and atmospheric profiles so a binning by magnetic elevation angle was also performed (results not shown) and

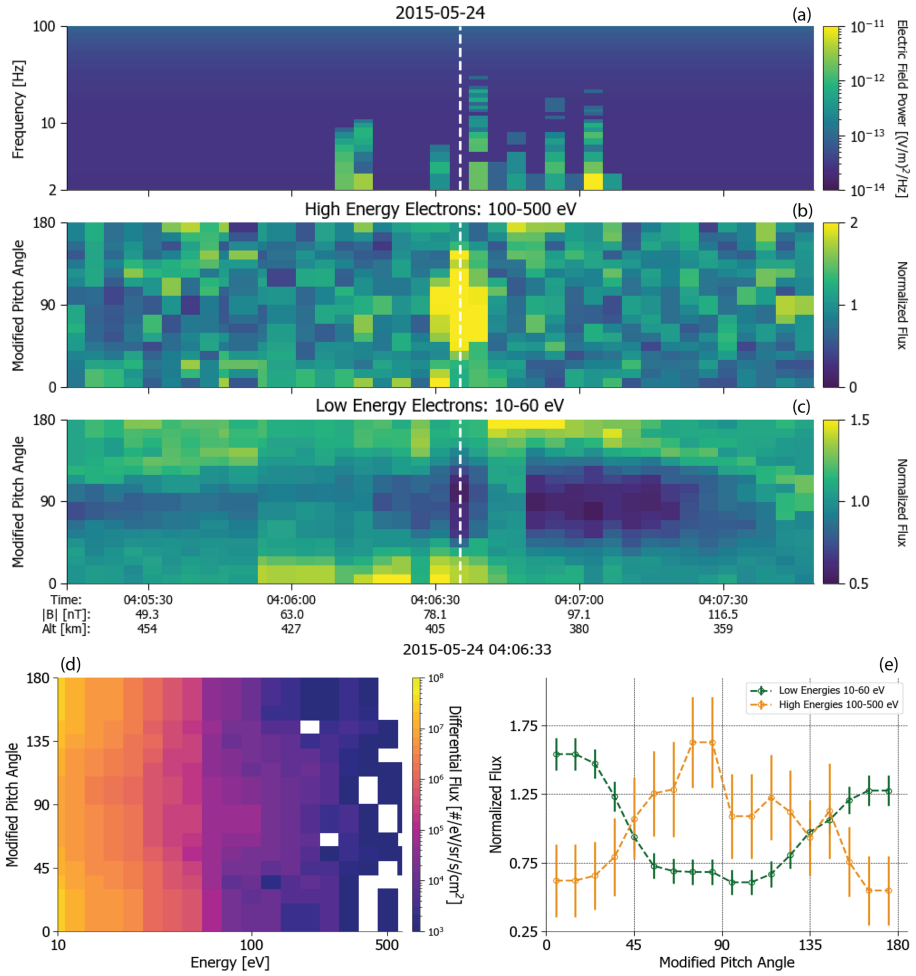

Figure 4. Time series of (a) electric wave power spectra from the Langmuir Probes and Waves instrument, (b) normalized high-energy photoelectron pitch angle distributions, and (c) normalized low-energy photoelectron pitch angle distributions. The white dashed line marks the observation at 04:06:33 with the complete energy-pitch angle distribution at this time shown in (d) and the normalized energy-averaged pitch angle distributions shown in (e).

the perpendicular peak exists on both horizontal and vertical field lines. The peak is narrower and more pronounced on vertical field lines; however, this can be explained by adiabatic motion.

5. Example Pad

Figure 4 plots an example MAVEN observation from 24 May 2015. These measurements took place on the dawn side of the planet (7 local time and 77° solar zenith angle) and over the strong crustal magnetic fields in the southern hemisphere (50°S, 150°E). Figures 4a–4c plot time series of the electric field wave power measured by the Langmuir Probes and Waves (LPW) instrument (Andersson et al., 2015) in passive mode, the normalized high-energy electron PAD, and the normalized low-energy electron PAD, respectively, over a ~3-min period. Note that Figures 4b and 4c have different color bar scales. The shape parameter is less than 1 in all directions (including trapped electrons) for this time period (photoelectrons dominate the low-energy distribution; see Xu et al., 2017, for details), indicating that these measurements all took place on closed crustal field structures.

As altitude increases (right to left of Figures 4a–4c), the low-energy electron source cone becomes deeper, in agreement with the general trend of modeling results and the statistical averages, from 04:07:50 to 04:06:45. The artificial diagonal line seen on top of this natural source cone is due to sunlight contamination. The high-energy electrons have more noise than the lower energies and are isotropic. During this time period, the magnetic elevation angle rotates from horizontal (~20° at 04:07:50) to near-vertical (~80° at 04:06:45).

Around 04:06:45, the low-energy electrons form a loss cone distribution, with more flux away from the planet than toward. The low-energy electrons then transition into a slightly asymmetric source cone with more flux toward the planet than away from 04:06:30 to 04:06:40. At the same time, the high-energy electrons have an intense flux increase at perpendicular pitch angles. The full energy-pitch angle distribution at 04:06:33 (indicated by the dashed white line) is shown in Figure 4d, and the normalized energy-averaged PAD is displayed in Figure 4e (vertical slices through Figures 4b and 4c). The exact values do not match as different normalization factors are used between Figures 4b and 4c and Figure 4e. Throughout these observations, LPW measured wave activity in the 2- to 30-Hz range. These frequencies lie between the local ion (<0.1 Hz) and electron gyrofrequency (>1,000 Hz) for this time period. At higher altitudes (>405 km), the high-energy electrons again are isotropic, the low-energy electrons have a source cone distribution, and the magnetic elevation angle rotates from vertical ~80° at 04:06:45) to horizontal (~20° at 04:05:10).

Coinciding with the acute flux increase of perpendicular high-energy electrons is a burst of electric field wave activity measured by LPW. Examining the magnetic field reveals many fluctuations across this time period; however, no distinct frequency stands out when a fast Fourier transform is performed. More analysis should be done on this time period to investigate the physics, but this is beyond the scope of this study and is left for future work. The purpose of this example is to demonstrate that the 2-year statistical averages of low- and high-energy PADs can be observed in any given observation.

6. Discussion and Conclusion

One process that could form the distributions observed for high-energy photoelectrons is magnetic pumping (Borovsky, 1986). Magnetic pumping is the result of two different waves effects on a particle population. A compressional magnetosonic wave will compress and relax the plasma due to $E \times B$ drift provided the frequency of the wave is small such that the first adiabatic invariant is conserved. If another wave (in cyclotron resonance with the particles) is also present and is actively pitch angle scattering the particle population, then the compression/relaxation cycle of the particles is interrupted and particles may gain energy from the compressional wave. At Mars, the compressional waves could come from pressure variations in the solar wind, causing the crustal fields to compress and relax. Weber et al. (2019) recently observed that during periods of high solar wind pressure, statistically, closed fields are seen less often, and draped fields are seen more often than during periods of low solar wind pressure. Due to the locality of the crustal fields, a local time effect is expected to be observed if magnetic pumping is the dominant process. A crustal field recently rotated onto the dayside will have experienced no pumping during night and no perpendicular peak should exist. In contrast, a crustal field on the dusk side will have experienced magnetic pumping throughout the day, and the effects should be maximized. No local time effect can be seen in the data (supporting information Figure S1), and therefore, we do not expect this to be the dominant process affecting the high-energy electron PADs.

Another process that could produce the observed distributions of high-energy photoelectrons on dayside-closed crustal field lines is adiabatic heating due to cross field drifts. On closed field lines, the gradient-curvature drift will be azimuthal, not radial, and would therefore not typically move electrons into regions of higher field strength. Provided the motional electric field and crustal field lines are in the correct orientation, solar wind electrons can $E \times B$ drift across field lines and onto a closed crustal field structure. However, Figures 2 and 3 are 2-year average distributions, and the angle between any individual crustal field line and the motional electric field is not constant enough for $E \times B$ drift to be the dominant process to form the flux peak at perpendicular pitch angles. Although a magnetosheath or external source of electrons can explain both the altitude dependence and the asymmetry in fluxes with respect to the planet, it seems unlikely that this is the dominant mechanism due to two issues. First, there is a lack of a known supply mechanism to the closed crustal field line, though wave-particle interactions in the sheath may scatter particles onto closed field lines. Second, the PADs of high-energy electrons on deep closed field lines ($|B| > 50\,\mathrm{nT}, B_{\mathrm{elev}} < 45°$, and altitude > 400 km to minimize collisional effects) still exhibit a perpendicular peak. Furthermore, whatever mechanism would be supplying external electrons would need to be local time independent as the perpendicular peak is seen immediately on the dawn side.

The most likely process that is producing the observed statistical distributions are wave-particle interactions. Whistler mode waves are an example of an energy-dependent scattering mechanism and have recently been observed at Mars (Harada et al., 2016; Fowler et al., 2018). These right-handed circularly polarized waves

occur between the local ion and electron gyrofrequency and will interact with different populations of electrons in energy-pitch angle space depending on the background plasma conditions (thermal electron density and magnetic field magnitude) and on the wave parameters (wave frequency and wave normal angle distributions). These waves can both pitch angle scatter and energy diffuse and are a good candidate process for producing the observed distributions. While pitch angle scattering may be occurring, the dominant process seems to be energization of locally gyrating low-energy electrons up to hundreds of electronvolts. Whistler waves are capable of preferentially energizing these electrons. The example shown in section 5 supports this explanation with both electric and magnetic variations observed between the local ion and electron gyrofrequency; however, it is by no means conclusive. Whistler mode waves are generated when a temperature anisotropy occurs ($T_{e\perp} > T_{e||}$). From a single spacecraft pass, it is difficult to determine the location of wave generation, direction of propagation, and region of interaction. For example, the increase in perpendicular flux may have generated whistler waves instead of being the result of them, as was observed by Fowler et al. (2018).

More work needs to be done in investigating the PADs of superthermal electrons on dayside-closed crustal field lines at Mars. Statistical averages from MAVEN measurements show that low-energy electrons behave as if collisional scattering and conservation of the first adiabatic invariant are the only processes that control their distribution. High-energy electrons on the other hand have an average distribution that cannot be explained by these two processes alone. A flux peak at perpendicular pitch angles indicates that a ubiquitous energization process is occurring on dayside-closed crustal field lines with wave-particle interactions being the most likely candidate. It is difficult at the moment to explain the asymmetry with respect to the planet with wave-particle interactions. An external source of electrons can explain this; however, this explanation suffers due to the lack of a known supply mechanism. The modification of electron PADs at these high energies is of direct importance to the energy budget in the Martian space environment. With ionization cross sections peaking at these energies for the main neutral species, this energization process may affect the ionosphere below. However, the energized electrons are outside the loss cone and low-energy electrons may still dominate the electron impact ionization due to higher fluxes. This will be especially important on the nightside as trapped electrons on closed field lines live longer (Shane et al., 2016) and will be able to deposit their energy deeper into the nightside ionosphere. Furthermore, these results show that there are unstudied physical processes occurring in the Martian space environment on dayside-closed crustal field lines.

Acknowledgments
This work was supported by the National Aeronautics and Space Administration (NASA) Grant NNX16AQ04G to the University of Michigan. The MAVEN project is funded by NASA through the Mars Exploration Program. All MAVEN data can be accessed through the Planetary Data System (https://pds.nasa.gov/).

References

Andersson, L., Ergun, R. E., Delory, G. T., Eriksson, A., Westfall, J., Reed, H., & Meyers, D. (2015). The Langmuir Probe and Waves (LPW) Instrument for MAVEN. *Space Science Reviews*, *195*(1), 173–198. https://doi.org/10.1007/s11214-015-0194-3

Borovsky, J. E. (1986). Magnetic pumping by magnetosonic waves in the presence of noncompressive electromagnetic fluctuations. *The Physics of Fluids*, *29*(10), 3245–3260. https://doi.org/10.1063/1.865842

Brain, D. A., Lillis, R. J., Mitchell, D. L., Halekas, J. S., & Lin, R. P. (2007). Electron pitch angle distributions as indicators of magnetic field topology near Mars. *Journal of Geophysical Research*, *112*, A09201. https://doi.org/10.1029/2007JA012435

Coates, A. J., Tsang, S. M. E., Wellbrock, A., Frahm, R. A., Winningham, J. D., Barabash, S., & Crary, F. J. (2011). Ionospheric photoelectrons: Comparing Venus, Earth, Mars and Titan. *Planetary and Space Science*, *59*(10), 1019–1027. https://doi.org/10.1016/j.pss.2010.07.016

Connerney, J. E. P., Espley, J., Lawton, P., Murphy, S., Odom, J., Oliversen, R., & Sheppard, D. (2015). The MAVEN magnetic field investigation. *Space Science Reviews*, *195*(1), 257–291. https://doi.org/10.1007/s11214-015-0169-4

Fowler, C. M., Andersson, L., Ergun, R. E., Harada, Y., Hara, T., Collinson, G., & Jakosky, B. M. (2018). MAVEN observations of solar wind-driven magnetosonic waves heating the Martian dayside ionosphere. *Journal of Geophysical Research: Space Physics*, *123*, 4129–4149. https://doi.org/10.1029/2018JA025208

Frahm, R. A., Sharber, J. R., Winningham, J. D., Wurz, P., Liemohn, M. W., Kallio, E., & Mckenna-Lawler, S. (2006). Locations of atmospheric photoelectron energy peaks within the Mars environment. *Space Science Reviews*, *126*(1), 389–402. https://doi.org/10.1007/s11214-006-9119-5

Frahm, R. A., Winningham, J. D., Sharber, J. R., Scherrer, J. R., Jeffers, S. J., Coates, A. J., & Dierker, C. (2006). Carbon dioxide photoelectron energy peaks at Mars. *Icarus*, *182*(2), 371–382. https://doi.org/10.1016/j.icarus.2006.01.014

Harada, Y., Andersson, L., Fowler, C. M., Mitchell, D. L., Halekas, J. S., Mazelle, C., & Jakosky, B. M. (2016). MAVEN observations of electron-induced whistler mode waves in the Martian magnetosphere. *Journal of Geophysical Research: Space Physics*, *121*, 9717–9731. https://doi.org/10.1002/2016JA023194

Itikawa, Y. (2002). Cross sections for electron collisions with carbon dioxide. *Journal of Physical and Chemical Reference Data*, *31*(3), 749–767. https://doi.org/10.1063/1.1481879

Jakosky, B. M., Lin, R. P., Grebowsky, J. M., Luhmann, J. G., Mitchell, D. F., Beutelschies, G., & Zurek, R. (2015). The Mars Atmosphere and Volatile Evolution (MAVEN) mission. *Space Science Reviews*, *195*(1), 3–48. https://doi.org/10.1007/s11214-015-0139-x

Khazanov, G. V., & Liemohn, M. W. (1995). Nonsteady state ionosphere-plasmasphere coupling of superthermal electrons. *Journal of Geophysical Research*, *100*(A6), 9669–9681. https://doi.org/10.1029/95JA00526

Khazanov, G. V., Liemohn, M. W., Gombosi, T. I., & Nagy, AF. (1993). Non-steady-state transport of superthermal electrons in the plasmasphere. *Geophysical Research Letters*, *20*(24), 2821–2824. https://doi.org/10.1029/93GL03121

Liemohn, M. W., Frahm, R. A., Winningham, J. D., Ma, Y., Barabash, S., Lundin, R., & Dierker, C. (2006). Numerical interpretation of high-altitude photoelectron observations. *Icarus*, *182*(2), 383–395. https://doi.org/10.1016/j.icarus.2005.10.036

Liemohn, M. W., Mitchell, D. L., Nagy, A. F., Fox, J. L., Reimer, T. W., & Ma, Y. (2003). Comparisons of electron fluxes measured in the crustal fields at Mars by the MGS magnetometer/electron reflectometer instrument with a B field-dependent transport code. *Journal of Geophysical Research*, *108*(E12), 5134. https://doi.org/10.1029/2003JE002158

Mitchell, D. L., Mazelle, C., Sauvaud, J. A., Thocaven, J. J., Rouzaud, J., Fedorov, A., & Jakosky, B. M. (2016). The MAVEN Solar Wind Electron Analyzer. *Space Science Reviews*, *200*(1), 495–528. https://doi.org/10.1007/s11214-015-0232-1

Shane, A. D., Xu, S., Liemohn, M. W., & Mitchell, D. L. (2016). Mars nightside electrons over strong crustal fields. *Journal of Geophysical Research: Space Physics*, *121*, 3808–3823. https://doi.org/10.1002/2015JA021947

Soobiah, Y. I. J, Wild, J. A., Beharrell, M. J., Barabash, S., Lillis, R. J., Mitchell, D. L., Coates, A. J., Winningham, J. D., & Frahm, R. A. (2014). Properties of a large-scale flux rope and current sheet region on the dayside of Mars: MGS MAG/ER and MEX ASPERA-3 ELS observations. *Icarus*, *242*, 297–315. https://doi.org/10.1016/j.icarus.2014.08.019

Thompson, W. R., Shah, M. B., & Gilbody, H. B. (1995). Single and double ionization of atomic oxygen by electron impact. *Journal of Physics B: Atomic, Molecular and Optical Physics*, *28*(7), 1321–1330. https://doi.org/10.1088/0953-4075/28/7/023

Weber, T., Brain, D., Mitchell, D., Xu, S., Connerney, J., & Halekas, J. (2017). Characterization of low-altitude nightside Martian magnetic topology using electron pitch angle distributions. *Journal of Geophysical Research: Space Physics*, *122*, 9777–9789. https://doi.org/10.1002/2017JA024491

Weber, T., Brain, D., Mitchell, D., Xu, S., Espley, J., Halekas, J., & Jakosky, B. (2019). The influence of solar wind pressure on Martian crustal magnetic field topology. *Geophysical Research Letters*, *46*, 2347–2354. https://doi.org/10.1029/2019GL081913

Xu, S., & Liemohn, M. W. (2015). Superthermal electron transport model for Mars. *Earth and Space Science*, *2*(3), 47–64. https://doi.org/10.1002/2014EA000043

Xu, S., Liemohn, M., Bougher, S., & Mitchell, D. (2016). Martian high-altitude photoelectrons independent of solar zenith angle. *Journal of Geophysical Research: Space Physics*, *121*, 3767–3780. https://doi.org/10.1002/2015JA022149

Xu, S., Liemohn, M. W., & Mitchell, D. L. (2014). Solar wind electron precipitation into the dayside Martian upper atmosphere through the cusps of strong crustal fields. *Journal of Geophysical Research: Space Physics*, *119*, 10,100–10,115. https://doi.org/10.1002/2014JA020363

Xu, S., Mitchell, D., Liemohn, M., Fang, X., Ma, Y., Luhmann, J., & Jakosky, B. (2017). Martian low-altitude magnetic topology deduced from MAVEN/SWEA observations. *Journal of Geophysical Research: Space Physics*, *122*, 1831–1852. https://doi.org/10.1002/2016JA023467

Xu, S., Thiemann, E., Mitchell, D., Eparvier, F., Pawlowski, D., Benna, M., & Mazelle, C. (2018). Observations and modeling of the Mars low-altitude ionospheric response to the 10 September 2017 X-class solar flare. *Geophysical Research Letters*, *45*, 7382–7390. https://doi.org/10.1029/2018GL078524

Xu, S., Weber, T., Mitchell, D. L., Brain, D. A., Mazelle, C., DiBraccio, G. A., & Espley, J. (2019). A technique to infer magnetic topology at Mars and its application to the terminator region. *Journal of Geophysical Research: Space Physics*, *124*, 1823–1842. https://doi.org/10.1029/2018JA026366